RSC Advances

ROYAL SOCIETY OF CHEMISTRY

www.rsc.org/advances

Sucrose-derived activated carbons: electron transfer properties and application as oxygen reduction electrocatalysts

Marta Nunes,[a] Inês M. Rocha,[b] Diana M. Fernandes,[a] Ana S. Mestre,[a,c] Cosme N. Moura,[d] Ana P. Carvalho,[c] Manuel F.R. Pereira[b] and Cristina Freire[a*]

[a] REQUIMTE/LAQV, Departamento de Química e Bioquímica, Faculdade de Ciências, Universidade do Porto, 4169-007 Porto, Portugal.

[b] Laboratório de Catálise e Materiais (LCM), Laboratório Associado LSRE-LCM, Departamento de Engenharia Química, Faculdade de Engenharia, Universidade do Porto, 4200-465 Porto, Portugal.

[c] Centro de Química e Bioquímica, Faculdade de Ciências, Universidade de Lisboa, 1749-016 Lisboa, Portugal.

[d] CIQ, Departamento de Química e Bioquímica, Faculdade de Ciências, Universidade do Porto, 4169-007 Porto, Portugal.

*Corresponding author: Dr. Cristina Freire; e-mail: acfreire@fc.up.pt

Tel.: +351 22 04020590; Fax: +351 22 0402 695

ABSTRACT

The development of carbon-based metal-free electrocatalysts for oxygen reduction reaction (ORR) is one of the most attractive topics in fuel cells field. Herein, we report the application of two sustainable sucrose-based activated carbons (ACs), denominated SC800 and SH800, as ORR electrocatalysts. In alkaline medium the ACs showed similar onset potentials at E_{onset} ≈ -0.20 V vs. Ag/AgCl (0.76 V vs. E_{RHE}), which are 0.06 V more negative than that observed for 20 wt% Pt/C used as reference. Higher diffusion-limiting current densities ($j_{L(-1.0\ V,\ 1600\ rpm)}$ = -3.44 mA cm^{-2}) were obtained for SH800 electrocatalyst, in contrast to SC800 ($j_{L(-1.0\ V,\ 1600\ rpm)}$ = -3.04 mA cm^{-2}). These differences can be related with their different textural properties. SH800 electrocatalyst revealed a higher specific surface area (A_{BET} ≈ 2500 m^2 g^{-1}), larger micropores (widths between 0.7 and 2 nm) and sponge-like morphology. Conversely, SC800 showed spherical shape, A_{BET} ≈ 1400 m^2 g^{-1} and narrow micropores with pore width < 0.7 nm. Both ACs were neither selective to 2- or 4-electron ORR processes, opposing to Pt/C which showed selectivity towards direct O_2 reduction to water. HS800 and SC800 showed very similar Tafel plots with two different slopes, with SH800 showing in both low and high currret densities the lowest values 53 / 171 mV dec dec^{-1} vs. 68 / 217 mV dec^{-1}. Furthermore, the ACs presented excellent tolerance to methanol, with SH800 electrocatalyst also showing greater long-term electrochemical stability than Pt/C electrocatalyst which are very important advantages.

The ACs-based electrocatalysts also showed ORR catalytic activity in acidic media, which makes them promising candidates for applications with acidic electrolytes (e.g. proton exchange fuel cells). In this case, E_{onset} = 0.06 V vs. Ag/AgCl (0.41 V vs. E_{RHE}) for SC800 and E_{onset} = -0.01 V vs. Ag/AgCl (0.34 V vs. E_{RHE}) for SH800, and the diffusion-limiting current densities are very similar for both ACs (j_L = -2.59/-2.76 mA

cm^{-2} at -1.3 V vs. Ag/AgCl, at 1600 rpm). SH800 and SC800 Tafel plots also showed two different slopes, but with higher values in both low and high current density regions, when compared with those obtained in alkaline medium; still SH800 continues to show the lowest slopes.

Keywords: Sucrose-derived activated carbons, Biomass, Cyclic voltammetry, Electrocatalysis, Oxygen reduction reaction.

1. INTRODUCTION

Carbon-based materials technologies have made remarkable progress in recent years. The wide availability, relative low cost, electrical conductivity and chemical and thermal stabilities of carbon materials makes them highly attractive candidates in a wide range of applications, namely as electrocatalysts or electrocatalysts supports for energy storage and conversion devices.[1,2]

Fuel cells are the most promising clean energy generation devices for which electrocatalysts play a key role.[3] This technology appeared as an alternative to counteract the depletion of fossil fuels and the growing threat of environmental pollution [4] and, nowadays, is recognized as an excellent power source due to its high efficiency and negligible pollutant emission.[5] Generally, the fuel cells devices are based on the electrocatalytic oxidation of a fuel (e.g. hydrogen and methanol) at the anode and the oxygen reduction reaction (ORR) at the cathode.[6] The ORR plays a crucial role in controlling the overall performance of fuel cells due to its slow kinetics,[4,7] requiring the use of an electrocatalyst in a high loading. Pt nanoparticles supported on carbon materials (Pt/C) are the most effective known ORR catalyst, leading to low ORR overpotential and large current densities, with selectivity toward a direct four-electron pathway.[8] Nevertheless, important drawbacks associated with the high prices, scarcity, poor long-term durability and possible Pt-deactivation by methanol crossover, have limited the large-scale application of fuel cells with Pt-based electrocatalysts.[9,10,11] To overcome these critical issues, research efforts have been made to developing alternative Pt-free ORR catalysts, with competitive ORR performance. In this context, carbon-based materials, with their versatile properties, appeared as ideal alternatives for ORR electrocatalysts and have been widely applied.

Several works have reported the application of graphite,[12] carbon nanotubes,[13,14,15] graphene,[16,17] ordered mesoporous carbons [9,18,19] and carbon nanoparticles [8] as metal-free ORR catalysts. Activated carbons, an amorphous carbonaceous material, also have been applied with this purpose. These materials take advantage of their high surface areas and well developed pore structure,[20] which are favourable conditions for a high ORR electrocatalytic activity, once increase the number of active sites exposed to the electrolyte.[4,5,21] However, a great number of commercial carbons are prepared from coal, a non-renewable raw material.[22] In this context, biomass emerged as a class of ideal starting materials for the green synthesis of carbon materials, once it is earth-abundant, readily available, cheap and environmental friendly.[3,23] The hydrothermal carbonization of biomass, via dehydration reactions in aqueous medium under mild conditions,[24] allows its conversion into valuable materials with fine tuning chemical structure and morphology.[21] The use of hydrothermal carbonization followed by activation was recently evaluated,[25] allowing to prepare superactivated carbons. The materials obtained are carbon- and oxygen-rich, due to the nature of biomass precursors,[22] which can constitute an advantage, since the ORR electrocatalytic activity and H_2O/H_2O_2 selectivity, could be influenced by the oxygen-containing groups.[14] Nevertheless, usually, the ORR conducted on carbon catalysts without doping, functionalization or substitution exhibits the two-plateau peroxide pathway.[1] Numerous studies have been published, reporting the application in ORR of carbon-based materials (undoped and doped) derived from several biomass sources, such as carbohydrates / polysaccharides (e.g. glucose [26,27,24,28] and chitin [29,30]), proteins from silk,[31,32] egg [33] and blood,[10] animal wastes,[34,35] plants,[3,5,21,36,37] fungus [23] and marine algae.[4,38] Some of these materials showed excellent ORR performance (assigned though E_{on} and j_L values), with catalytic activities competitive with the Pt/C electrocatalyst, but

greater stability and tolerance to methanol poisoning is still a prior demand.[4,21, 38] Nevertheless, these results constitute a tremendous advantage and encourage further studies with this type of biomass-derived materials.

This work reports the application of two sustainable activated carbons (AC) prepared from a sucrose-derived hydrochar,[25,39] denoted by SC800 and SH800, as ORR electrocatalysts. Their ORR electrocatalytic activities were explored in alkaline and acidic media using cyclic and linear sweep voltammetry, and their stabilities and tolerances to methanol poisoning effects in alkaline media were also evaluated by chronoamperometry and cyclic voltammetry, respectively. Complementary characterization, included ACs surface chemical composition by X-ray photoelectron spectroscopy and electron transfer properties of the AC-based modified electrodes in the presence of selected redox probes, $[Fe(CN)_6]^{3-/4-}$, $[Ru(NH_3)_6]^{3+/2+}$ and $Eu^{3+/2+}$. Dependency between the electron transfer properties and materials C/O ratios with multiple concurrent effects, have already been observed in studies involving graphite oxides,[40] graphene-type materials [41,42] and carbon quantum dots,[43] evaluating the electrochemical response of materials in the presence of selected redox probes.

To the best of our knowledge, this is the first paper reporting the application of ACs metal-free ORR electrocatalysts derived from sucrose. Di Noto *et. al* already presented ORR electrocatalysts whose preparation included the use of sucrose;[44,45,46] nonetheless, the resulting materials included metallic nanoparticles (Pt, Ni and Rh) deposited in carbon nitrides.

2. EXPERIMENTAL SECTION

2.1 Reagents and solvents

All reagents used in activated carbons preparation, namely sucrose (Analar Normapur, > 90 %), potassium carbonate (K_2CO_3, Aldrich, 99 %) and potassium hydroxide (KOH, Panreac, 85 %) were used as received. Potassium chloride (KCl, Merck, ≥ 99.5 %), potassium hexacianoferrate (III) ($K_3[Fe(CN)_6]$, Merck, ≥ 99 %), aminoruthenium (III) chloride ($[Ru(NH_3)_6]Cl_3$, Aldrich, 98.0 %), europium (III) chloride hexahydrate ($EuCl_3.6H_2O$, Aldrich, 99.9 %), potassium hydroxide (KOH, Riedel-de-Häen), sodium sulfate (Na_2SO_4, Prolabo, 99.5 %), sulfuric acid (H_2SO_4, Merck, 95-97 %), Nafion (Aldrich, 5 wt% solution in lower aliphatic alcohols and water), ethanol (Panreac, 99.8 %) and methanol (Fisher Scientific, > 99.99 %) were used as received. The 20 wt% Pt/C standard catalyst was prepared by incipient wetness impregnation method. The active metal precursor, $H_2PtCl_6.6H_2O$, dissolved in water, was slowly added to the carbon support, Printex80. During 24 hours, the sample was dried in an oven at 373 K. The dried sample was annealed at T = 523 K, during 1 h under N_2 and reduced during 3 h under H_2.

2.2 Preparation of materials

The sucrose-derived activated carbons were prepared by a hydrothermal carbonization of sucrose solution followed by a chemical activation, as described in literature.[39] Briefly, 15 mL of a 1.5 mol dm^{-3} sucrose aqueous solution was introduced in a Teflon-line stainless steel autoclave during 5 h at 190 ºC. The obtained powder (hydrochar S) was washed with distilled water and acetone and dried (60 ºC). For chemical activation, 1 g of hydrochar was impregnated under stirring on a solution with 4 g of K_2CO_3 or KOH during 2 h and then dried. Activation was performed at 800 ºC in a horizontal furnace (Thermolyne, model 21100) for 1 h under a N_2 flow of 5 cm^3 s^{-1} (10 ºC min^{-1}). After cooling, the materials were thoroughly washed with distilled water

until pH 7 was reached, dried overnight at 100 ºC and stored. The materials are labelled as S (hydrochar) followed by H or C for KOH or K_2CO_3, respectively, and the activation temperature, resulting in designations SH800 and SC800.

2.3 Materials characterization

The textural characterization of the sucrose-derived activated carbons was made by N_2 and CO_2 adsorption isotherms at -196 ºC and 0 ºC, respectively. The N_2 isotherms were performed in an automatic equipment (Micromeritics ASAP 2010) while the CO_2 adsorption isotherms were obtained on a conventional volumetric apparatus equipped with a MKS-Baratron (310BHS-1000) pressure transducer (0–133 kPa). Before the isotherm acquisition the samples (≈ 50 mg) were outgassed overnight at 120 ºC under a vacuum (pressure < 10-2 Pa). From N_2 adsorption data, the apparent surface area, A_{BET}, and microporosity were evaluated through, respectively, the BET equation ($0.05 < p/p_0 < 0.15$) [47] and α_S method, taking as reference the isotherm reported by Rodríguez-Reinoso *et al.* [48]. The micropore size distributions were obtained from the CO_2 adsorption isotherms, according to the method described by Pinto *et al.* [49].

The X-ray photoelectron spectroscopy (XPS) measurements were performed at CEMUP (Porto, Portugal), in a Kratos AXIS Ultra HSA spectrometer using a monochromatic Al Kα radiation (1486.7 eV). The XPS spectra were deconvoluted with the XPSPEAK 4.1 software, using non-linear least squares fitting routine after a Shirley-type background subtraction. To correct possible deviations caused by electric charge of the samples, the C 1s band at 284.6 eV was taken as the internal standard. The surface atomic percentages were calculated from the corresponding peak areas, using the sensitivity factors provided by the manufacturer.

2.4 Evaluation of the ORR electrocatalytic activity

The ORR performance of each electrocatalyst was evaluated at room temperature in a three electrode compartment cell. The cyclic voltammetry (CV) and linear sweep voltammetry (LSV) measurements were carried out using an Autolab PGSTAT 302N potentiostat/galvanostat (EcoChimie B.V.), controlled by NOVA v1.10 software. A rotating disk electrode (RDE) of glassy carbon (3 mm of diameter, Metrohm) was used as working electrode, an Ag/AgCl (3 mol dm^{-3} KCl, Metrohm) as reference electrode and a glassy carbon rod (2 mm of diameter, Metrohm) as auxiliary electrode. The modified-electrodes were prepared by the following procedure: 1 mg of SH800 or 20 wt% Pt/C catalysts or 2 mg of SC800 were dispersed ultrasonically in 1 mL of a Nafion/ethanol (1:9 v/v) mixture for 30 min. Then, a 3 μL drop of the select dispersion were deposited in the RDE surface and dried under an air flux, yielding an electrocatalyst loading of 99.05 μg cm^{-2}. Prior to modification, the electrode was conditioned by a polishing/cleaning procedure, using diamond pastes of 6, 3 and 1 μm (MetaDi II, Buehler) and aluminium oxide of particle size 0.3 μm (Buehler), on a microcloth polishing pad (BAS Bioanalytical Systems Inc.). To finish, the electrode was rinsed and sonicated for 10 min in ultra-pure water.

The electrochemical tests were accomplished in N_2- or O_2-saturated (purged for 30 min before the measurements) 0.1 mol dm^{-3} KOH or H_2SO_4/Na_2SO_4 buffer solution with pH= 2.5 (prepared by mixing appropriate amounts of a 0.2 mol dm^{-3} H_2SO_4 solution with a 0.5 mol dm^{-3} Na_2SO_4 solution). CV experiments were conducted at the scan rate of 0.005 V s^{-1} and the LSV at 0.005 V s^{-1} for different rotation speeds from 400 to 3000 rpm; chronoamperometry measurements were performed at E = -0.6 V vs Ag/AgCl and 1600 rpm during 20 000 s. The methanol-tolerance evaluation was performed by CV at 0.010 V s^{-1}. The ORR current was obtained by subtracting the

current measured in N_2-saturated electrolytes from the current measured in O_2-saturated electrolyte.

The onset potential (E_{onset}), defined as the potential at which the O_2 reduction reaction starts, was calculated as described in literature. [6] In order to facilitate the comparison with the literature, the E_{onset} values determined vs. Ag/AgCl were converted to the reversible hydrogen electrode (RHE) scale according to the Nernst equation:

$$E_{RHE} = E_{Ag/AgCl} + 0.059\ pH + E^{o}_{Ag/AgCl} \quad (1)$$

where E_{RHE} is the converted potential vs. RHE, $E^{o}_{Ag/AgCl}$ = 0.1976 at 25 ºC and $E_{Ag/AgCl}$ is the experimentally measured potential against Ag/AgCl reference. [50]

LSV data was analysed though Koutecky-Levich (K-L) equation (2). The number of electrons transferred per O_2 molecule (n_{O2}) in the ORR process was calculated from the slopes of the K-L plot:[21,38]

$$\frac{1}{j} = \frac{1}{j_L} + \frac{1}{j_k} = \frac{1}{B\omega^{1/2}} + \frac{1}{j_k} \quad (2)$$

where j is the experimentally measured current density, j_L is the diffusion-limiting current density, j_k is the kinetic current density and ω is the angular velocity; B is related to the diffusion limiting current density expressed by the Equation (3):

$$B = 0.2\ n_{O2}\ F (D_{O_2})^{2/3} v^{-1/6} C_{O_2} \quad (3)$$

where F is the Faraday constant (96 485 C mol^{-1}), C_{O_2} is the bulk concentration of O_2, v is the kinematic viscosity of the electrolyte and D_{O_2} is the diffusion coefficient of O_2. The constant 0.2 is adopted when the rotating speed is in rpm. In 0.1 mol dm^{-3} KOH media C_{O_2}= 1.15×10^{-3} mol dm^{-3}, v = 0.008977 cm^2 s^{-1} and D_{O_2}= 1.95×10^{-5} cm^2 s^{-1},[13] while in H_2SO_4/Na_2SO_4 buffer media C_{O_2}= 1.26×10^{-3} mol dm^{-3}, v = 0.01 cm^2 s^{-1} and D_{O_2}= 1.77×10^{-5} cm^2 s^{-1}.[51] The Tafel plots (E_{RHE} vs. log i_k) for oxygen reduction kinetics

were obtained after the measured currents in LSV were corrected for diffusion to give the kinetic currents. The mass transport correction was made using the diffusion-limiting current density j_L, calculated by combination of equations (2) and (3), since it could not be obtained directly from the LSV. The obtained current density j_k was multiplied by the geometric area of the GCE disk (A = 0.07067 cm^2) yielding i_k, which was normalized for the total deposited mass of ACs for SC800 and SH800 electrocatalysts; in the case of Pt/C, i_k was normalized on Pt mass existing in the deposited Pt/C mass. [52]

2.5 Electrochemical characterization of modified electrodes

CV measurements were carried out using an Autolab PGSTAT 30 potentiostat/galvanostat (EcoChimie B.V.), controlled by a GPES software. The studies were performed on a conventional three-electrode compartment cell, using a glassy carbon electrode, GCE, (3 mm of diameter, BAS, MF-2012) as working electrode, a platinum wire (7.5 cm, BAS, MW-1032) as auxiliary electrode and the Ag/AgCl (sat. KCl) (BAS, MF-2052) as reference electrode. The cell was enclosed in a grounded Faraday cage and all studies were carried out at room temperature in deaerated solutions.

To prepare the modified electrodes, the activated carbons (SC800 or SH800, 1 mg) were dispersed in N,N'-dimethylformamide (DMF, 1 mL) and sonicated for 20 min. Then, a 3 μL drop of the selected material dispersion was deposited onto the GCE surface, followed by solvent evaporation under an air flux. Prior to modification, the GCE electrode was conditioned as described above.

CV of the redox probes $K_3[Fe(CN)_6]$, $[Ru(NH_3)_6]Cl_3$ or $EuCl_3.6H_2O$ were performed using solutions 1.0×10^{-3} mol dm^{-3} in KCl 1.0 mol dm^{-3}. All solutions were

prepared using ultra-pure water (resistivity 18.2 MΩ cm at 25°C, Millipore). According with the electrochemical probe used, the potential was cycled between 0.75 and -0.25 V, 0.20 and -0.50 V or -0.10 and -1.00 V, at several scan rates from 0.010 to 0.500 V s^{-1}. Each experiment was repeated until obtain concordant results.

The electroactive surface areas were determined using the Randles-Sevcik equation, Equation (4), assuming that the electrode process is controlled by diffusion:

$$i_{pc} = 2.69 \times 10^5 \, n^{3/2} \, A \, D_x^{1/2} \, C \, v^{1/2} \quad (4)$$

where n is the number of electrons involved in the process (1 in this case), A is the electrode surface area (cm^2), D_x the diffusion coefficient (6.30×10^{-6} cm^2 s^{-1} for $[Fe(CN)_6]^{3-/4-}$,[53] 6.20×10^{-6} cm^2 s^{-1} for $[Ru(NH_3)_6]^{3+/2+}$ [54] and 6.50×10^{-6} cm^2 s^{-1} for $Eu^{3+/2+}$ [55]), C the concentration of the specie (mol cm^{-3}), v is the scan rate (V s^{-1}) and i_{pc} the intensity of the cathodic peak current (A). [56]

The heterogeneous electron transfer (HET) rates were evaluated by Nicholson's method, that relates the ΔE_p to a dimensionless charge transfer parameter Ψ and, consequently, to k_{HET} (HET rate constant), through Equation (5) [57,58]

$$\Psi = \frac{k_{HET}}{(\pi D_x \frac{nFv}{RT})^{1/2}} \quad (5)$$

where R is the gas constant, F is Faraday's constant, T is the temperature (25 ºC) and the remaining symbols have the significance described above. The Ψ values were estimated from ΔE_p, according with the tabulated values by Nicholson.[57]

3. RESULTS AND DISCUSSION

3.1 Activated carbons characterization

The N_2 adsorption-desorption isotherms (Figure 1(a)) of the sucrose-derived activated carbons belong to type I in the IUPAC classification, [59] being characteristic of

materials with a well-developed micropore network. Carbon SH800, obtained by KOH activation, presents the more developed microporous structure and the rounder off knee of its N_2 isotherm is indicative of the presence of larger micropores (supermicropores). This sample presents a sponge-like morphology [39]. Sample SC800, activated with K_2CO_3, has lower N_2 adsorption capacity and the isotherm presents a sharper knee revealing the existence of narrower micropores, but retains the spherical morphology of the hydrochar [39]. The textural parameters of the materials (Table 1) are in accordance with the analysis of the shape of the curves. The apparent surface area of carbon SH800 attains more than 2400 $m^2\ g^{-1}$ while for carbon SC800 is 1375 $m^2\ g^{-1}$, and the total microporous volume of SH800 is almost the double of that presented by SC800 (1.08 versus 0.62 $cm^3\ g^{-1}$). As expected from the configuration of the N_2 isotherms, the data from the α_s method reveal that the micropore network of carbon SH800 is composed exclusively by larger micropores (supermicropores – widths between 0.7 and 2 nm), while carbon SC800 presents similar amounts of ultra (widths < 0.7 nm) and supermicropores. Further characterization of the sucrose-derived activated carbons by micropore size distributions (Figure 1(b)), assessed by fitting CO_2 adsorption data at 0 ^oC to the method described by Pinto *et al.* [49], corroborates the assumptions made above. Carbon SH800 has a bimodal micropore size distribution with pores mainly in the supermicropore region and a very large amount of pores with widths between 1.3 and 2 nm, whereas sample SC800 presents a monomodal distribution centered at ≈ 0.7 nm and negligible volume of pores with widths > 1.5 nm.

Figure 1

Table 1

The SH800 and SC800 sucrose-derived activated carbons were further characterized by XPS; the obtained survey spectra for both materials are depicted in Figure S1 in Supporting Information (SI). The deconvoluted high resolution XPS spectra of SH800 in C 1s and O 1s regions are showed in Figure 2 with the indication of the binding energies and the equivalent spectra for SC800 are depicted in Figure S2 in SI.

Figure 2

In the XPS survey spectra, both activated carbons do not show any peak due to any catalytic active metal; besides C and O, the spectra show residual traces of Al 2p, Si 2p and K 2p. Consequently, the ORR electrocatalytic activity described below for both SC800 and SH800 activated carbons relates to metal-free electroctalysts.

For both samples, the C 1s high-resolution spectra were deconvoluted with five peaks: a main peak at 284.6 eV assigned to graphitic carbon (sp^2), a peak at 285.9 / 286.0 eV attributed to sp^3 hybridized carbon, a peak at 287.1 / 287.3 eV assigned to C-O, a peak at 288.6 / 288.8 eV related to C=O and a peak at 289.8 / 290.2 eV ascribed to –COO bonds.[60] The O 1s spectra were fitted with two peaks, at 532.0 and 533.4 eV, assigned to C=O and C-O environments, respectively.[20,61]

The surface atomic percentages of each element in both materials are summarized in Table 2. The results showed that both materials have very similar C% ≈ 82 (≈ 65 mmol g^{-1}) and O% ≈ 18 (≈ 14 mmol g^{-1}), indicating that they are surface enriched in oxygen-containing groups. For SC800, C% is similar to the compositional data provided by the elemental analysis previously published (81.2 wt% of C, 67.6 mmol g^{-1}) [25] while, for SH800, the C% obtained by XPS is higher than the reported by elemental analysis

(74.5 wt%, 62.0 mmol g^{-1}),[25] suggesting for the latter material inhomogeneity between the carbon and oxygen bulk and surface compositions.

Table 2

3.2 Electrocatalytic activity for ORR

LSV measurements with rotating disk electrode (RDE) were performed to investigate the ORR performances of the prepared activated carbons electrocatalysts. The ORR activities were tested in alkaline media (0.1 mol dm^{-3} KOH) and acidic media (H_2SO_4/Na_2SO_4 buffer solution, pH 2.5). For comparison, the standard 20 wt% Pt/C was also measured in ORR. The results obtained in alkaline media are depicted in Figure 3.

Figure 3

Figure 3 (a) presents the CVs obtained for SC800 and SH800 modified electrodes in N_2- and O_2- saturated solutions. In N_2-saturated solution no electrochemical processes are observed, while in O_2-saturated solution all materials exhibited an irreversible electrochemical process indicative of their electrocatalytic activity for ORR. The SC800 modified electrode showed two cathodic peaks, at E_{pc} = -0.26 and E_{pc} = -0.44 V vs. Ag/AgCl (0.70 and 0.52 V vs. E_{RHE}, respectively), and the SH800 showed only one defined cathodic peak, at E_{pc} = -0.28 V vs. Ag/AgCl (0.68 V vs. E_{RHE}).

Figure 3 (b) shows the ORR polarization plots of the prepared catalysts, the 20 wt% Pt/C and the bare GCE. The RDE voltammograms for the ORR on individual bare GCE and SC800, SH800 and Pt/C modified electrodes, at rotation rates from 400 to

3000 rpm, are depicted in Figure S3. Both activated carbons-based electrocatalysts showed similar onset potentials (E_{onset} = -0.19 and -0.20 V vs. Ag/AgCl (0.77 and 0.76 V vs. E_{RHE}) for SC800 and SH800, respectively), but higher diffusion-limiting current densities ($j_{L(-1.0\ V,\ 1600\ rpm)}$ = -3.44 mA cm^{-2}) were obtained for SH800 electrocatalyst, in contrast to SC800 ($j_{L(-1.0\ V,\ 1600\ rpm)}$ = -3.04 mA cm^{-2}). These differences can be related to the distinct morphologies, surface area and micropore size distributions of the two materials. The material SH800 revealed a higher specific surface area, A_{BET}, around 2500 $m^2\ g^{-1}$, presenting larger micropores and widths between 0.7 and 2 nm (Table 1), and sponge-like morphologies; on the other hand, SC800 showed a spherical shape, with $A_{BET} \approx$ 1400 $m^2\ g^{-1}$ and narrow micropores with pore width < 0.7 nm. [25] Several works [4,5,21] have reported that high surface areas and large pore structures are favourable conditions for ORR, since it would favour mass transport of the electrolyte, allowing for a higher catalytic current density, assuming mass transfer limited currents. In this context, the better performance (higher current densities) exhibited by SH800 is a consequence of its larger pores that enable the electrolyte solution to flow into/out of the catalyst more easily.

The results indicated a superior ORR performance of the activated carbons modified electrodes in comparison to the bare GCE (E_{onset} = -0.33 V vs. Ag/AgCl (0.63 V vs. E_{RHE}), $j_{L(-1.0\ V,\ 1600\ rpm)}$ = -2.18 mA cm^{-2}), with onset potential at less negative values and higher current densities, which demonstrate the advantage of the electrode modification. On the other hand, the results obtained with activated carbons are near to those obtained with 20 wt% Pt/C (E_{onset} = -0.14 V vs. Ag/AgCl (0.82 V vs. E_{RHE}), $j_{L(-0.9\ V,\ 1600\ rpm)}$ = -3.91 mA cm^{-2}), with a difference of ΔE_{onset} = 0.06 V between the onset potentials of Pt/C and ACs-based modified electrodes.

In the context of other biomass-based carbon materials (usually, highly porous materials) for ORR, [4,5,26,27,28] the majority refers to heteroatom doped materials (N and S), with the undoped analogues being equivalent to those prepared in this work. The E_{onset} values obtained for SH800 and SC800 (-0.20 V vs. Ag/AgCl) compare well or are less negative to those obtained for undoped and N-doped glucose-derived carbon aerogels (E_{onset} = -0.1, -0.20, -0.30 V vs Ag/AgCl) when they used as electrocatalysts in alkaline medium [5,26,27,28].

The ORR kinetic parameters were analysed by the Koutecky-Levich (K-L) plots (j^{-1} *vs.* $\omega^{-1/2}$) at various potentials, using the RDE voltammograms. The slopes of their linear fit lines were used to estimate the number of electrons transferred per oxygen molecule (n_{O2}), although it is recognised that the high surface areas and high degree of porosity may interfere in the transport properties of the active species (O_2 and reaction intermediates) in the electrolyte. From the corresponding K-L plots (in the range -0.5 to -1.0 V vs. Ag/AgCl), Figure S4, it can be seen that the data exhibited good linearity, although the different straight lines exhibited different slopes, anticipating a variation in the n_{O2} values with potential. From Figure 3 (c) it is possible to verify that the estimated number of electrons transferred is very similar between the SC800 and SH800 catalysts, increasing as the potential become more negative, revealing that the electrocatalysts are not selective for either the 2 (indirect reduction through peroxide pathway) or 4 electron processes (direct O_2 reduction): at E = -0.5 V vs. Ag/AgCl, the electrocatalysts are involved in a n_{O2} = 1.85-1.93 electrons process, shifting to n_{O2} = 3.03-3.12 electrons at E = -1.0 V vs. Ag/AgCl. These values are bigger than that displayed by GCE (n_{O2} = 1.70 electrons, at E = -1.0 V vs. Ag/AgCl), being closer to the $\tilde{n}_{O2}$ = 3.94 electrons estimated for 20 wt% Pt/C, for which a 4 electron processes is observed. The obtained n_{O2} values and its dependence with potential are also very similar to what is observed

when glucose-derived carbon materials are used as ORR electrocatalysts in alkaline medium. [26,27,28]

In alkaline medium, oxygen indirect reduction through peroxide pathway envolves a two reaction steps mechanism of two electrons: in the first reaction, O_2 is reduced to HO_2^- ($O_2 + H_2O + 2e^- \rightarrow HO_2^- + HO^-$) and, in the second reaction, the intermediates are reduced to H_2O/HO^- ($HO_2^- + H_2O + 2e^- \rightarrow 3\ HO^-$). On opposite, the direct O_2 reduction reaction corresponds to a single reaction involving four electrons, where O_2 is directly reduced to H_2O/HO^- ($O_2 + 2\ H_2O + 4e^- \rightarrow 4\ HO^-$). [1]

Further information on ORR kinetics and mechanism can be obtained from the Tafel plots for both ACs and Pt/C, Figure 4. Both ACs showed very similar Tafel plots with two different slopes with similar values: 53 /68 mV dec^{-1} in low current density region and 171 / 217 mV dec^{-1} in high current density region, for SH800 and SC800, respectively. As expected, the highest performance electrocatalyst SH800 showed lower slopes. The Pt/C electrocatalyst showed a different Tafel plot with different slope values (85 / 192 mV dec^{-1}), suggesting a different mechanism in which Pt is the active site. [62] The ORR mechanism in undoped carbon materials that present oxygen groups is still a matter of debate and only few papers address the topic, for pyrolytic graphite, CNTs and graphene oxide.[1] The identified oxygen containing groups with ORR activity are the so-called quinone-like groups, that are capable of O_2 adsorbing and efficiently mediate the first $2e^-$ reduction of O_2 to HO_2^- and subsequent reduction of the intermediates to HO^-. [63,64,65] The ACs-based electrocatalysts have very similar oxygen contents and although XPS is not able to discrimination the oxygen-type groups and respective quantities, the similarity of the Tafel slopes and profiles suggests that the different electrocatalytic activities may be not directly related to the type of oxygen groups, but to the different

textural properties, namely the higher surface area and larger microporous of SH800 comparative to SC800.

Figure 4

An important parameter in fuel-cells where methanol is used as fuel, as in direct methanol fuel-cells, is the tolerance of the catalyst to fuel molecules, that may pass across the membrane from the anode to the cathode and to poison the catalyst.[38,21] The platinum-based electrocatalysts have the disadvantage of selectivity to methanol oxidation, which completely subdues the ORR and reduces the current output.[4] Therefore, methanol tolerance tests were performed by cyclic voltammetry, with SC800, SH800 modified electrodes and standard Pt/C for comparison. The CVs obtained in O_2-saturated 0.1 mol dm^{-3} KOH solutions, in the presence and absence of methanol (1.0 mol dm^{-3}), for SC800, SH800 and 20 wt% Pt/C modified electrodes are depicted in Figures 5 (a), (b) and (c), respectively. In the presence of methanol, the Pt/C electrocatalyst showed an anodic peak at E_{pa} = -0.17 V vs. Ag/AgCl attributed to methanol oxidation, that overlaps the ORR and reflects the low tolerance of Pt to methanol, as expected. On the contrary, there were no significant changes in the electrochemical response of SC800 and SH800 electrocatalysts after the introduction of methanol, demonstrating their high selectivity for oxygen reduction against the electro-oxidation of methanol and, consequently, the excellent tolerance towards crossover methanol effect. These results make SC800 and SH800 materials promising electrocatalysts to be applied in fuel cells, especially in direct methanol fuel cells.

Figure 5

Another important parameter is the stability / durability of the ORR electrocatalysts. Thus, the long-term stability of the SC800, SH800 and Pt/C electrocatalysts were evaluated by chronoamperometric measurements at E = -0.60 V vs Ag/AgCl in O_2-saturated 0.1 mol dm^{-3} KOH solution at 1600 rpm, and the results are present in Figure 5 (d). After 20 000 s, the 20 wt% Pt/C chronoamperogram showed a current decay to 68.0 %. At the end of the same period of time, the SC800 current declined to 53.9 %, while the SH800 showed a current decay only to 72.9 %. These data revealed that the activated carbons have different electrochemical stabilities, with the SH800 being the most stable ORR electrocatalysts. These differences can be related to the combination of distinct morphologies, surface areas and porosity: the SH800 electrocatalyst showing higher surface area and larger pores, will have higher number of active sites (quinone-like groups) that will be easily accessed by the O_2/HO_2^-/electrolyte, leading to higher durability.[25] Furthermore, SH800 also showed to be more stable than the standard Pt/C catalysts, which is a promisor result. This could be a consequence of the migration and aggregation of Pt particles caused by continuous potential, contrasting to the higher stability carbon materials structure.

Figure 6 shows the results obtained in acidic media (H_2SO_4/Na_2SO_4 buffer solution, pH 2.5). The CVs obtained in N_2- and O_2-saturated solutions are depicted in Figure 6 (a). The activated carbons-based electrocatalysts showed ORR electrocatalytic activity also in acidic media, exhibiting cathodic peaks at E_{pc} = -0.16 V and E_{pc} = -0.11 V vs. Ag/AgCl (0.18 V and 0.24 V vs. E_{RHE}), for SC800 and SH800, respectively. This is a key result because usually carbon materials are known to be inactive or present lower ORR activity in acidic media.[21] The ORR catalytic activity in acidic media is also very important for proton exchange fuel cells which required acid electrolytes.[66]

Interestingly, other electrochemical processes (at E = -0.72 / 0.28 V for SC800 and E = -0.73 / 0.06 or 0.20 V for SH800 vs. Ag/AgCl) were also observed in both N_2- and O_2-saturated solutions, which can be related to other redox processes inherent of the activated carbon materials in acidic media and not directly related to ORR.

Figure 6

The ORR polarization plots for all materials are depicted in Figure 6 (b) and the individual RDE voltammograms can be observed in Figure S5 in SI. Similarly to the results obtained in alkaline media, also in acidic media, the electrodes modified with SC800 and SH800 showed higher ORR performance than the bare GCE, exhibiting onset potentials at more positive values (E_{onset} = 0.06 V vs. Ag/AgCl (0.41 V vs. E_{RHE}) for SC800 and E_{onset} = -0.01 V vs. Ag/AgCl (0.34 V vs. E_{RHE}) for SH800). These onset potential values are considerably more negative than those obtained with the Pt/C modified electrode (E_{onset} = 0.41 V vs. Ag/AgCl (0.76 V vs. E_{RHE})), resulting in a ΔE_{onset} = 0.35-0.42 V. The declining of the carbon materials performance in acidic media, when compared with Pt/C, can be associated to some active sites deactivation, for example protonation of oxygen ORR active groups which become inactive and non-accessible for O_2 adsorption.[6] Furthermore, all modified electrodes displayed identical ORR diffusion-limiting current densities (j_L = -2.68, -2.59 and -2.76 mA cm^{-2} for bare GCE, SC800 and SH800, respectively (at E = -1.3 V vs. Ag/AgCl), and j_L = -2.78 for 20 wt% Pt/C (at E = -0.3 V vs. Ag/AgCl), at 1600 rpm. In comparison with other biomass-based carbon materials (N- and S-doped) reported as ORR electrocatalysts, [5,26] the E_{onset} values obtained for SC800 and SH800 (0.06 and -0.01 V vs. Ag/AgCl, respectively) are less positive than those obtained for N-doped glucose-based carbons materials (0.20 -

0.50 V vs. Ag/AgCl). [5,26] K-L plots are presented in Figure S6 in SI and the number of electrons transferred per O_2 molecule and its variation according with the applied potential can be observed in Figure 6 (c) for all electrocatalysts. The SC800 and SH800 electrocatalyst continue to present similar n_{O2} values, but with some variation with the applied potential: at E = -1.3 V, n_{O2} = 2.26 for SC800, n_{O2} = 2.31 for SH800 and n_{O2} = 1.80 for the bare GCE. At this experimental conditions, Pt/C electrocatalyst presented n_{O2} = 3.27 (at -0.3 V).

Tafel plots for ACs, depicted in Figure S7 in SI, also presented two different slopes: 227 / 1001 mV dec^{-1} for SC800 and 145 / 561 mV dec^{-1} for SH800, in low and high current density regions, respectively. Globally, the results suggest lower electrocatalytic activity and different ORR mechanisms compared to the equivalent data in alkaline medium; nevertheless SH800 still showed the lowest slopes and consequently highest ORR performance. Moreover, Pt/C electrocatalyst showed lower Tafel slopes (81 / 504 mV dec^{-1}) than for ACs, indicating highest catalytic activity. [62]

3.3 Electrochemical characterization of the modified electrodes

Further electrochemical characterization was performed to the SC800- and SH800-modified electrodes, in order to evaluate other possible applications. The CVs of SC800 and SH800 activated carbon-modified electrodes and bare GCE, in KCl 1.0 mol dm^{-3}, are compared in Figure 7 (a). Rectangular voltammograms are observed for both activated carbons, suggesting a capacitive behaviour for these materials; [38,67] this was proved by the linear plots of current intensities (measured at E = 0.0 V) as a function of scan rates (from v = 0.5 to 0.06 V s^{-1}) (*i vs. v*) for both materials, as depicted in Figure S8. Both ACs show high capacitive values of similar magnitudes, although SC800 exhibited a higher value, 233.2 μF, compared to 143.3 μF for SH800.

Figure 7

The electrochemical properties of activated carbons were explored in the presence of the redox probes $[Fe(CN)_6]^{3-/4-}$, $[Ru(NH_3)_6]^{3+/2+}$ and $Eu^{3+/2+}$, Figures 7 (b), (c) and (d), respectively. The CVs for $[Ru(NH_3)_6]^{3+/2+}$ using the SC800 and SH800 modified electrodes, Figure 7 (c), showed one pair of redox peaks at E_{pc} = -0.20 V/ E_{pa} = -0.13 V vs. Ag/AgCl that are assigned to Ru^{3+}/Ru^{2+} electronic transfer; furthermore, the CVs profiles are very similar to that observed when using GCE, indicating that the redox probe does not interact significantly with the modified electrodes. The anodic to cathodic peak-to-peak separations (ΔE) obtained for both modified electrodes are very similar (ΔE_p= 0.072 V for SC800 and ΔE = 0.071 V for SH800 vs. Ag/AgCl), which are in agreement with the insensitivity of the $[Ru(NH_3)_6]^{3+/2+}$ probe to surface defects and oxygen-containing groups.[42] With the $[Fe(CN)_6]^{3-/4-}$ redox probe (Figure 7 (b)), the CVs profiles for both SC800 and SH800 modified electrodes are also similar to the bare

GCE, with a cathodic peak at $E_{pc} \approx 0.24$ V and an anodic peak at $E_{pa} \approx 0.32$ V (Fe^{3+}/Fe^{2+} electron transfer), and with ΔE = 0.083 and 0.080 V vs. Ag/AgCl for SC800 and SH800, respectively. The similarity between peak potentials and ΔE values for the modified and bare electrodes are also indicative of a non-significant interaction between the redox probe and the modified electrodes surface.

The CV of $Eu^{3+/2+}$ probe using the bare GCE, Figure 7 (d), showed the electrochemical process associated with Eu^{3+}/Eu^{2+} electron transfer, with E_{pc} = -0.67 V and E_{pa} = -0.50 V and ΔE = 0.172 V vs. Ag/AgCl. In the CVs of activated carbons-modified electrodes it is also possible to observe the redox processes due to Eu^{3+}/Eu^{2+}, but the peak potentials are shifted: E_{pc} values are shifted to less negative potentials whereas the E_{pa} values are shifted to more negative potentials (E_{pc} = -0.64 V / E_{pa} = -0.54 V for SC800 and E_{pc} = -0.63 V /E_{pa} = -0.55 V for SH800 vs. Ag/AgCl). These variations are reflected in a decrease in ΔE_p values, compared to the GCE: ΔE = 0.097 V for SC800 and ΔE = 0.080 V for SH800 vs. Ag/AgCl. These results indicate a different interaction of the redox probe with each modified electrode through the oxygen groups, since the probe can, in this case, bind directly to the carbon-oxygen groups. [42] Thus, in the CV of redox probe using GCE the electrochemical process due to Eu^{3+}/Eu^{2+} is dominated by the europium species in solution. On the other hand, in CVs of the redox probe using the activated carbons-modified electrodes, the observed electrochemical process due to Eu^{3+}/Eu^{2+} may also have contributions from the europium species attached to the oxygen groups in carbon materials. Although the activated carbons showed similar surface oxygen content (O% from XPS), the material SH800 have a higher bulk oxygen content associated with a higher surface area and well developed porosity. In this context, the lower ΔE value compared to SC800-modified

electrode is compatible with a higher % of adsorbed Eu^{3+}/Eu^{2+} due to the highest bulk oxygen content.

In the experimental timescale employed (scan rates in the range 0.01 to 0.5 V s^{-1}) both E_{pc} and E_{pa} varied less than 0.010 V for $[Fe(CN)_6]^{3-/4-}$, 0.010 V (SC800) and 0.005 V (SH800) for $[Ru(NH_3)_6]^{3+/2+}$ and 0.030 V (SC800) and 0.009 (SH800) for $Eu^{2+}/^{3+}$ vs. Ag/AgCl. Figure 8 shows the plots of log i_p versus log v for bare GCE and SC800 and SH800 modified electrodes. All plots have slopes around 0.50, indicating predominantly diffusion-controlled processes.[56] In addition, the ratios i_{pa}/i_{pc} are close to one in all cases (see Table S1 in SI).

Figure 8

The electroactive surface area of bare GCE and SC800 and SH800 modified electrodes were determined from CVs of 1×10^{-3} mol dm^{-3} $K_3[Fe(CN)_6]$, $[Ru(NH_3)_6]Cl_3$ and $EuCl_3.6H_2O$ in KCl 1.0 mol dm^{-3} (Figures S9, S10 and S11 in SI, respectively), using the Equation (4); the A values are summarized in Table 3.

Table 3

For all probes, the electroactive areas determined for SC800 and SH800 are larger than for bare electrode, indicating that the modification with these materials provide a more conductive pathway for the electron transfer of tested probes. The areas determined using the $[Fe(CN)_6]^{3-/4-}$ and $[Ru(NH_3)_6]^{3+/2+}$ probes are very similar for each modified electrode and, even, identical between the SC800 and SH800 materials. With the $Eu^{2+}/^{3+}$ probe, the areas determined for activated carbon materials remains very

similar between them, but are smaller than the areas calculated with the other two probes.

The HET rate constants, k_{HET}, were determined through Equation (5) for SC800 and SH800 modified electrodes for all redox probes solutions. The higher k_{HET} values were obtained for $[Ru(NH_3)_6]^{3+/2+}$, k_{HET} = 1.23 × 10^{-2} cm^2 s^{-1}, for both modified electrodes, reflecting the lowest ΔE_p values. For $[Fe(CN)_6]^{3-/4-}$, k_{HET} are similar for both modified electrodes, k_{HET} = 6.20 × 10^{-3} and 6.82 × 10^{-3} cm^2 s^{-1} for SC800 and SH800 modified electrodes, respectively. In the case of $Eu^{2+/3+}$ probe, the SC800 modified electrode showed a k_{HET} = 4.72 × 10^{-3} cm^2 s^{-1}, which is different from that of SH800 (k_{HET} = 6.30 × 10^{-3} cm^2 s^{-1}).

4. CONCLUSIONS

The SC800 and SH800 activated carbons derived from sucrose were characterized by XPS, revealing that both have similar surface C% and O%, although SH800 showed higher oxygen bulk contents. The ACs showed different textural properties: SH800 revealed a higher specific surface area (A_{BET} ≈ 2500 m^2 g^{-1}), larger micropores (widths between 0.7 and 2 nm) and sponge-like morphology, whereas SC800 showed spherical shape, A_{BET} ≈ 1400 m^2 g^{-1} and narrow micropores with pore width < 0.7 nm.

Both activated carbons showed ORR electrocatalytic activity in alkaline media, with similar onset potentials (E_{onset}≈ -0.20 V vs. Ag/AgCl) but higher current densities were obtained for SH800, which was explained by its more well-developed porosity and higher surface area. Both electrocatalysts revealed excellent tolerance to methanol, with SH800 presenting inclusive, greater long-term electrochemical stability than the state-of-the-art Pt/C electrocatalyst. The sucrose-derived activated carbons also showed ORR

catalytic activity in acidic media, although with medium ORR performances, but making them as promising for applications in proton exchange fuel cells.

All of these results, allied with the fact of both electrocatalysts are made from a renewable biomass, highlight the potential of these porous activated carbons (mainly SH800, due to its superior stability in alkaline media) towards electrocatalysis for energy conversion. Moreover, although the 4-electrons mechanism (selectivity to H_2O) is known to be favourable for ORR in order to have higher efficiencies, a process with H_2O_2 selectivity (2-electrons mechanism), can also be useful for the co-generation of hydrogen peroxide and electricity under the same electrochemical reaction conditions; consequently, the sustainable approach used offers a versatile protocol for carbon-based electrocatalysts application.

ACKNOWLEDGMENTS

This work was co-financed by Fundação para a Ciência e a Tecnologia (FCT) and FEDER under Programme PT2020 (Projects UID/QUI/50006/2013, UID/MULTI/00612/2013 and UID/EQU/50020/2013). MN (SFRH/BD/79171/2011), IR (SFRH/BPD/108490/2015), DF (SFRH/BPD/74877/2010) and ASM (SFRH/BPD/86693/2012) also thank FCT for their grants.

REFERENCES

1. D. W. Wang and D. S. Su, *Energy Environ. Sci.*, 2014, **7**, 576-591.
2. P. Trogadas, T. F. Fuller and P. Strasser, *Carbon*, 2014, **75**, 5-42.
3. H. M. Zhang, Y. Wang, D. Wang, Y. B. Li, X. L. Liu, P. R. Liu, H. G. Yang, T. C. An, Z. Y. Tang and H. J. Zhao, *Small*, 2014, **10**, 3371-3378.
4. M. Y. Song, H. Y. Park, D. S. Yang, D. Bhattacharjya and J. S. Yu, *ChemSusChem*, 2014, **7**, 1755-1763.
5. J. P. Li, S. G. Wang, Y. Q. Ren, Z. H. Ren, Y. J. Qiu and J. Yu, *Electrochim. Acta*, 2014, **149**, 56-64.
6. N. Daems, X. Sheng, I. F. J. Vankelecom and P. P. Pescarmona, *J. Mater. Chem. A*, 2014, **2**, 4085-4110.

7. H. J. Lu, Y. Li, L. Q. Zhang, H. N. Li, Z. X. Zhou, A. R. Liu, Y. J. Zhang and S. Q. Liu, *RSC Adv.*, 2015, **5**, 52126-52131.
8. G. Panomsuwan, N. Saito and T. Ishizaki, *Phys. Chem. Chem. Phys.*, 2015, **17**, 6227-6232.
9. G. J. Tao, L. X. Zhang, L. S. Chen, X. Z. Cui, Z. L. Hua, M. Wang, J. C. Wang, Y. Chen and J. L. Shi, *Carbon*, 2015, **86**, 108-117.
10. C. Z. Guo, W. L. Liao, Z. B. Li and C. G. Chen, *Carbon*, 2015, **85**, 279-288.
11. R. Silva, G. M. Pereira, D. Voiry, M. Chhowalla and T. Asefa, *RSC Adv.*, 2015, **5**, 49385-49391.
12. A. Shen, Y. Zou, Q. Wang, R. A. W. Dryfe, X. Huang, S. Dou, L. Dai and S. Wang, *Angewandte Chemie (International ed. in English)*, 2014, **53**, 10804-10808.
13. G. Tuci, C. Zafferoni, A. Rossin, A. Milella, L. Luconi, M. Innocenti, L. T. Phuoc, D. V. Cuong, P. H. Cuong and G. Giambastian, *Chem. Mat.*, 2014, **26**, 3460-3470.
14. H. J. Zhang, H. L. Li, C. C. Deng, B. Zhao and J. H. Yang, *ECS Electrochem. Lett.*, 2015, **4**, 5.
15. M. Vikkisk, I. Kruusenberg, S. Ratso, U. Joost, E. Shulga, I. Kink, P. Rauwel and K. Tammeveski, *RSC Adv.*, 2015, **5**, 59495-59505.
16. J. C. Wang, R. G. Ma, Z. Z. Zhou, G. H. Liu and Q. Liu, *Sci Rep*, 2015, **5**, 9.
17. J. J. Wu, L. L. Ma, R. M. Yadav, Y. C. Yang, X. Zhang, R. Vajtai, J. Lou and P. M. Ajayan, *ACS Appl. Mater. Interfaces*, 2015, **7**, 14763-14769.
18. J. J. Shi, X. J. Zhou, P. Xu, J. L. Qiao, Z. W. Chen and Y. Y. Liu, *Electrochim. Acta*, 2014, **145**, 259-269.
19. J. L. Li, Z. L. Li, J. H. Tong, C. G. Xia and F. W. Li, *RSC Adv.*, 2015, **5**, 70010-70016.
20. Y. Chen, S. R. Zhai, N. Liu, Y. Song, Q. D. An and X. W. Song, *Bioresour. Technol.*, 2013, **144**, 401-409.
21. P. Chen, L. K. Wang, G. Wang, M. R. Gao, J. Ge, W. J. Yuan, Y. H. Shen, A. J. Xie and S. H. Yu, *Energy Environ. Sci.*, 2014, **7**, 4095-4103.
22. W. J. Si, J. Zhou, S. M. Zhang, S. J. Li, W. Xing and S. P. Zhuo, *Electrochim. Acta*, 2013, **107**, 397-405.
23. S. Y. Gao, H. Fan and S. X. Zhang, *J. Mater. Chem. A*, 2014, **2**, 18263-18270.
24. A. Jung, S. Han, T. Kim, W. J. Cho and K. H. Lee, *Carbon*, 2013, **60**, 307-316.
25. A. S. Mestre, E. Tyszko, M. A. Andrade, M. Galhetas, C. Freire and A. P. Carvalho, *RSC Adv.*, 2015, **5**, 19696-19707.
26. S. A. Wohlgemuth, R. J. White, M. G. Willinger, M. M. Titirici and M. Antonietti, *Green Chem.*, 2012, **14**, 1515-1523.
27. N. Brun, S. A. Wohlgemuth, P. Osiceanu and M. M. Titirici, *Green Chem.*, 2013, **15**, 2514-2524.
28. S. A. Wohlgemuth, T. P. Fellinger, P. Jaker and M. Antonietti, *J. Mater. Chem. A*, 2013, **1**, 4002-4009.
29. M. K. Rybarczyk, M. Lieder and M. Jablonska, *RSC Adv.*, 2015, **5**, 44969-44977.
30. H. R. Yuan, L. F. Deng, X. X. Cai, S. G. Zhou, Y. Chen and Y. Yuan, *RSC Adv.*, 2015, **5**, 56121-56129.
31. T. Iwazaki, R. Obinata, W. Sugimoto and Y. Takasu, *Electrochem. Commun.*, 2009, **11**, 376-378.
32. T. Iwazaki, H. S. Yang, R. Obinata, W. Sugimoto and Y. Takasu, *J. Power Sources*, 2010, **195**, 5840-5847.
33. K. L. Wang, H. Wang, S. Ji, H. Q. Feng, V. Linkov and R. F. Wang, *RSC Adv.*, 2013, **3**, 12039-12042.
34. J. Zhang, S. Y. Wu, X. Chen, K. Cheng, M. Pan and S. C. Mu, *RSC Adv.*, 2014, **4**, 32811-32816.
35. Z. Zhang, H. Li, Y. X. Yang, J. L. Key, S. Ji, Y. Y. Ma, H. Wang and R. F. Wang, *RSC Adv.*, 2015, **5**, 27112-27119.

36. H. M. Zhang, J. Y. Chen, Y. B. Li, P. R. Liu, Y. Wang, T. C. An and H. J. Zhao, *Electrochim. Acta*, 2015, **165**, 7-13.
37. X. J. Liu, Y. C. Zhou, W. J. Zhou, L. G. Li, S. B. Huang and S. W. Chen, *Nanoscale*, 2015, **7**, 6136-6142.
38. F. F. Liu, H. L. Peng, C. H. You, Z. Y. Fu, P. Y. Huang, H. Y. Song and S. J. Liao, *Electrochim. Acta*, 2014, **138**, 353-359.
39. A. S. Mestre, C. Freire, J. Pires, A. P. Carvalho and M. L. Pinto, *J. Mater. Chem. A*, 2014, **2**, 15337-15344.
40. C. H. A. Wong, Z. Sofer and M. Pumera, *Chem.-Eur. J.*, 2015, **21**, 8435-8440.
41. J. G. S. Moo, A. Ambrosi, A. Bonanni and M. Pumera, *Chem.-Asian J.*, 2012, **7**, 759-770.
42. S. M. Tan, A. Ambrosi, C. K. Chua and M. Pumera, *J. Mater. Chem. A*, 2014, **2**, 10668-10675.
43. C. S. Lim, K. Hola, A. Ambrosi, R. Zboril and M. Pumera, *Electrochem. Commun.*, 2015, **52**, 75-79.
44. V. Di Noto, E. Negro, R. Gliubizzi, S. Gross, C. Maccato and G. Pace, *J. Electrochem. Soc.*, 2007, **154**, B745-B756.
45. V. Di Noto, E. Negro, K. Vezzu, L. Toniolo and G. Pace, *Electrochim. Acta*, 2011, **57**, 257-269.
46. V. Di Noto, E. Negro, S. Polizzi, K. Vezzu, L. Toniolo and G. Cavinato, *Int. J. Hydrog. Energy*, 2014, **39**, 2812-2827.
47. S. J. Gregg and K. S. W. Sing, *Adsorption, Surface Area and Porosity*, Academic Press Inc., London, 1982.
48. F. Rodriguez-Reinoso, J. M. Martin-Martinez, C. Prado-Burguete and B. McEnaney, *J. Phys. Chem.*, 1987, **91**, 515-516.
49. M. L. Pinto, A. S. Mestre, A. P. Carvalho and J. Pires, *Ind. Eng. Chem. Res.*, 2010, **49**, 4726-4730.
50. S. Hoang, S. W. Guo, N. T. Hahn, A. J. Bard and C. B. Mullins, *Nano Lett.*, 2012, **12**, 26-32.
51. A. Mani and V. I. Birss, *J. Electroanal. Chem.*, 2012, **687**, 102-110.
52. E. Negro, K. Vezzu, F. Bertasi, P. Schiavuta, L. Toniolo, S. Polizzi and V. Di Noto, *ChemElectroChem*, 2014, **1**, 1359-1369.
53. D. M. Fernandes, M. Costa, C. Pereira, B. Bachiller-Baeza, I. Rodriguez-Ramos, A. Guerrero-Ruiz and C. Freire, *J. Colloid Interface Sci.*, 2014, **432**, 207-213.
54. G. P. Keeley, A. O'Neill, N. McEvoy, N. Peltekis, J. N. Coleman and G. S. Duesberg, *J. Mater. Chem.*, 2010, **20**, 7864-7869.
55. M. C. Henstridge, E. Laborda, Y. J. Wang, D. Suwatchara, N. Rees, A. Molina, F. Martinez-Ortiz and R. G. Compton, *J. Electroanal. Chem.*, 2012, **672**, 45-52.
56. A. J. F. Bard, L. R., *Electrochemical Methods, Fundamentals and Applications*, New York, 2001.
57. R. S. Nicholson, *Analytical Chemistry*, 1965, **37**, 1351-1355.
58. A. Ambrosi and M. Pumera, *Chem.-Eur. J.*, 2013, **19**, 4748-4753.
59. M. Thommes, K. Kaneko, A. V. Neimark, J. P. Olivier, F. Rodriguez-Reinoso, J. Roquerol and K. S. W. Sing, *Pure Appl. Chem.*, 2015, **87**, 1051-1069.
60. X. L. Wu, L. L. Chen, S. Xin, Y. X. Yin, Y. G. Guo, Q. S. Kong and Y. Z. Xia, *ChemSusChem*, 2010, **3**, 703-707.
61. M. E. Lipinska, S. L. H. Rebelo, M. F. R. Pereira, J. Gomes, C. Freire and J. L. Figueiredo, *Carbon*, 2012, **50**, 3280-3294.
62. Y. J. Zhang, K. Fugane, T. Mori, L. Niu and J. H. Ye, *J. Mater. Chem.*, 2012, **22**, 6575-6580.
63. D. H. Deng, L. Yu, X. L. Pan, S. Wang, X. Q. Chen, P. Hu, L. X. Sun and X. H. Bao, *Chem. Commun.*, 2011, **47**, 10016-10018.

64. S. Wang, S. M. Dong, J. Wang, L. X. Zhang, P. X. Han, C. J. Zhang, X. G. Wang, K. J. Zhang, Z. G. Lan and G. L. Cui, *J. Mater. Chem.*, 2012, **22**, 21051-21056.
65. M. N. Zhang, Y. M. Yan, K. P. Gong, L. Q. Mao, Z. X. Guo and Y. Chen, *Langmuir*, 2004, **20**, 8781-8785.
66. G. L. Lu, H. S. Yang, Y. L. Zhu, T. Huggins, Z. J. Ren, Z. N. Liu and W. Zhang, *J. Mater. Chem. A*, 2015, **3**, 4954-4959.
67. A. Ambrosi, H. L. Poh, L. Wang, Z. Sofer and M. Pumera, *ChemSusChem*, 2014, **7**, 1102-1106.

CAPTIONS TO FIGURES

Figure 1. (a) N_2 adsorption–desorption isotherms at -196 ºC, closed symbols are the desorption points; (b) micropore size distributions of the activated carbons (adapted from ref. [39]).

Figure 2. Deconvoluted high-resolution XPS spectra for SH800: (a) C 1s and (b) O 1s.

Figure 3. ORR results in KOH 0.1 mol dm^{-3}: (a) CVs of the as-prepared catalysts in N_2- and O_2-saturated solutions at 0.005 V s^{-1}, (b) LSV using RDE in O_2-saturated solution at 1600 rpm and 0.005 V s^{-1} and (c) number of electrons transferred per O_2 molecule (n_{O2}) at several potential values.

Figure 4. ORR Tafel plots for SC800 and SH800 activated carbons and 20 wt% Pt/C, obtained from LSV data in Figure 3 (b); current intensities normalized to the mass of each electrocatalyst deposited on electrode (see experimental section).

Figure 5. CVs for ORR in O_2-saturated 0.1 mol dm^{-3} KOH with and without methanol (1.0 mol dm^{-3}) for SC800 (a), SH800 (b) and 20 wt% Pt/C (c); relative *j*-t chronoamperometric responses of catalysts at E = -0.60 V and 1600 rpm, in O_2-saturated 0.1 mol dm^{-3} KOH solution (d).

Figure 6. ORR results in H_2SO_4/Na_2SO_4 (pH 2.5): (a) CVs of the as-prepared catalysts in N_2- and O_2-saturated solutions at 0.005 V s^{-1}, (b) LSV using RDE in O_2-saturated solution at 1600 rpm and 0.005 V s^{-1} and (c) number of electrons transferred per O_2 molecule (n_{O2}) at several potential values.

Figure 7. CVs of bare GCE and SC800 and SH800 modified electrodes, at the scan rate of 0.05 V s^{-1} in: (a) KCl 1.0 mol dm^{-3} supporting electrolyte and in the presence of

1.0×10^{-3} mol dm^{-3} redox probe in KCl 1.0 mol dm^{-3}: (b) $K_3[Fe(CN)_6]$; (c) $[Ru(NH_3)_6]Cl_3$ (d) and $EuCl_3.6H_2O$.

Figure 8. Plots of log i_{pc} and i_{pa} vs. log ν of bare GCE, SC800 and SH800 modified electrodes in: (a) $[Fe(CN)_6]^{3-/4-}$, (b) $[Ru(NH_3)_6]^{3+/2+}$ and (c) $Eu^{2+}/^{3+}$ solutions 1.0×10^{-3} mol dm^{-3} in KCl 1.0 mol dm^{-3}.

Figure 1.

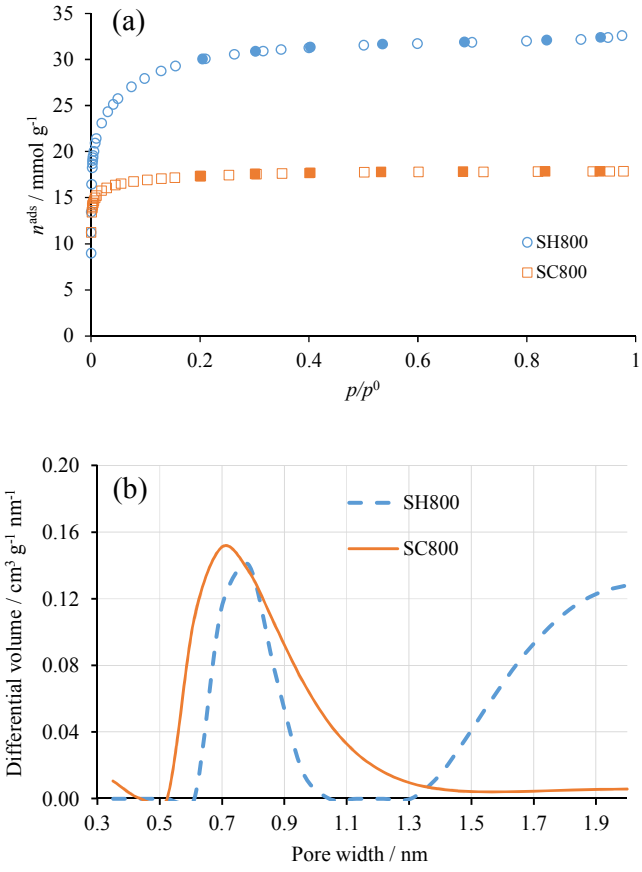

Figure 2.

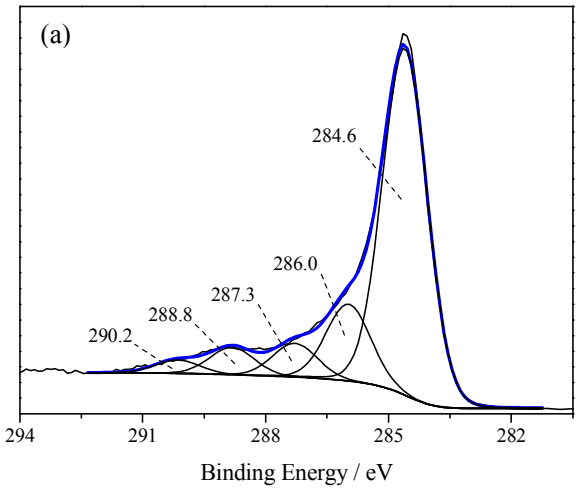

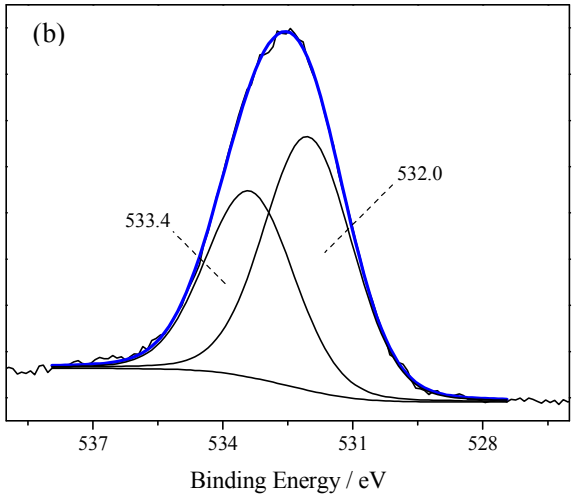

Figure 3.

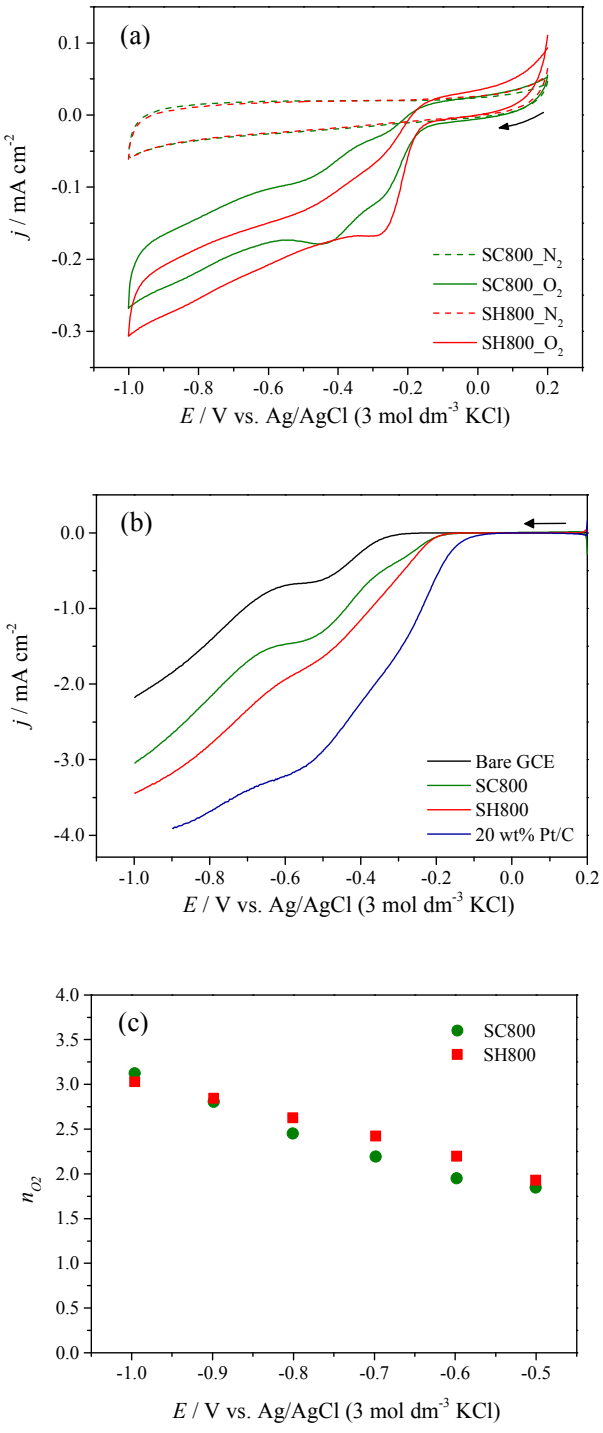

Figure 4.

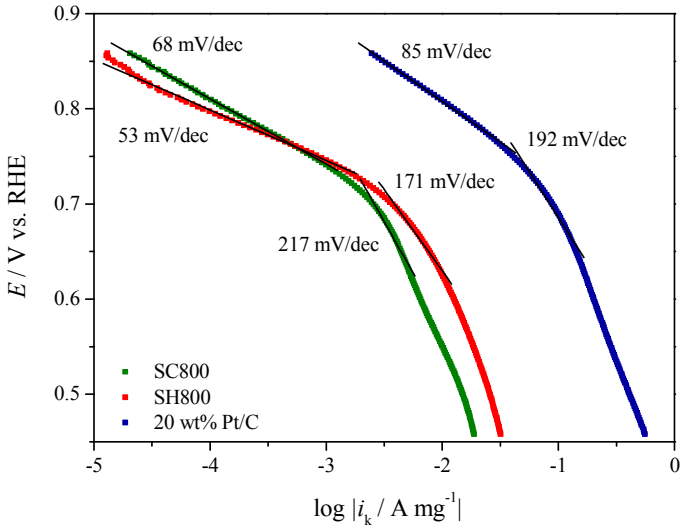

Figure 5.

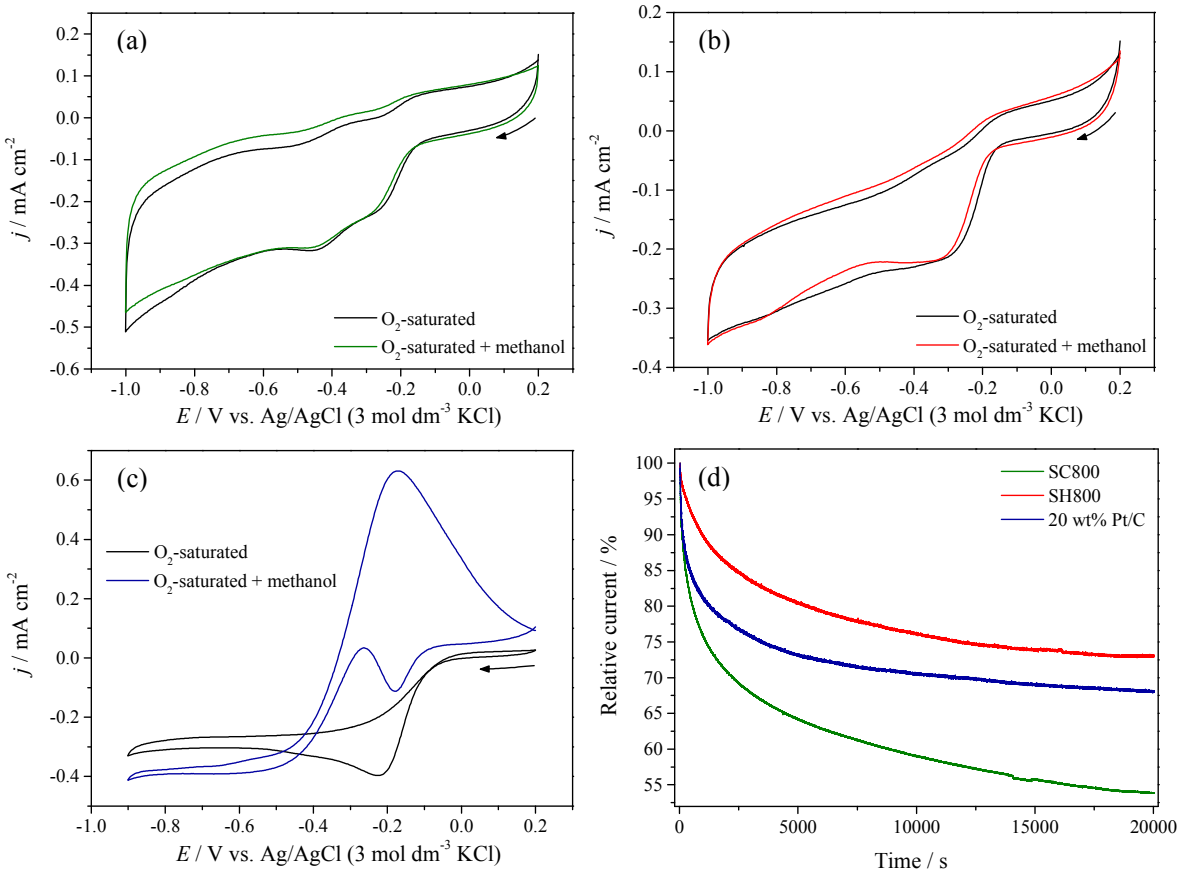

Figure 6.

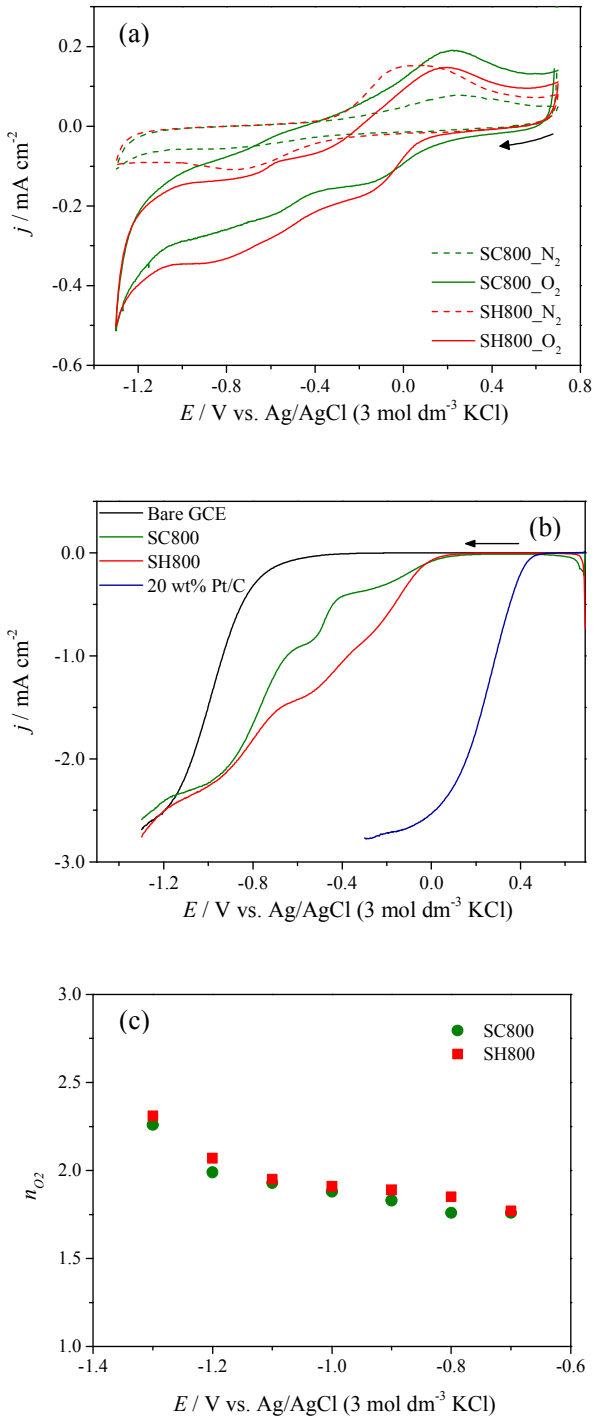

Figure 7.

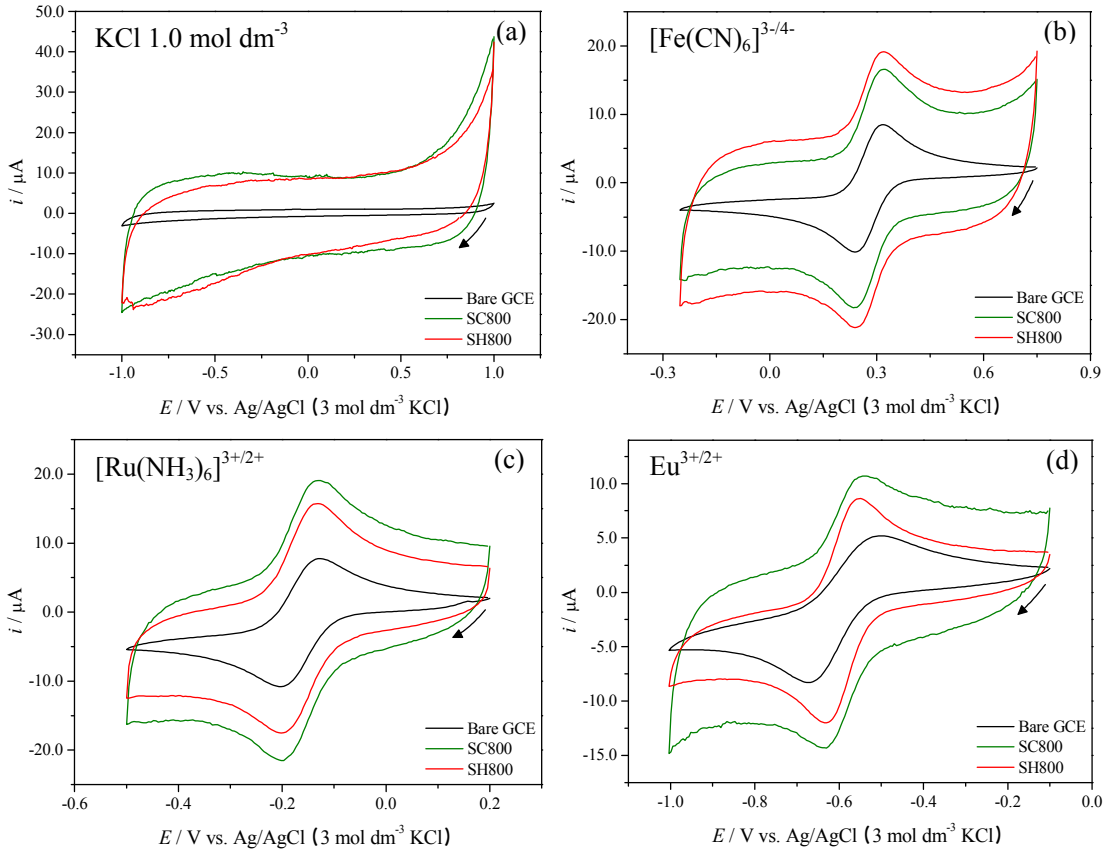

Figure 8.

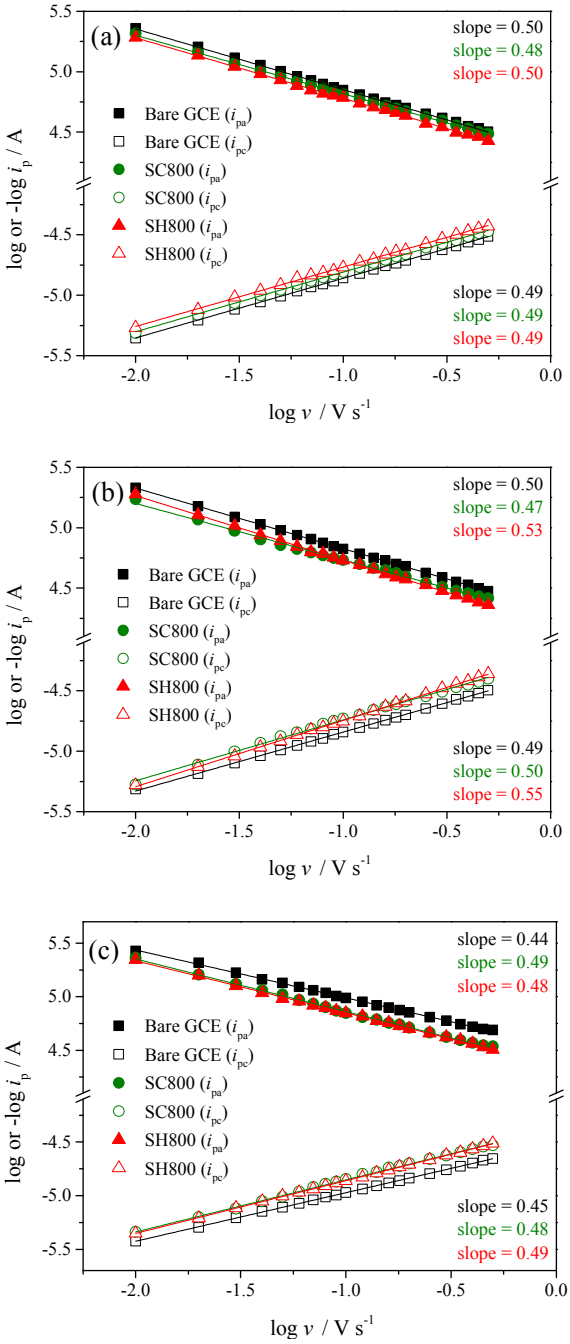

Table 1: Textural properties of the sucrose-derived activated carbons (adapted from ref. [39]).

Sample	A_{BET} ($m^2 g^{-1}$)	V_{total} [a] ($cm^3 g^{-1}$)	V_{meso} [b] ($cm^3 g^{-1}$)	α_s Method [c, d, e]		
				$V_{\alpha\ total}$ ($cm^3 g^{-1}$)	$V_{\alpha\ ultra}$ ($cm^3 g^{-1}$)	$V_{\alpha\ super}$ ($cm^3 g^{-1}$)
SH800	2431	1.14	0.06	1.08	0.00	1.08
SC800	1375	0.63	0.01	0.62	0.35	0.27

[a] evaluated at $p/p^0 = 0.975$ in the N_2 adsorption isotherms at -196 ºC.
[b] difference between V_{total} and $V_{\alpha\ total}$.
[c] $V_{\alpha\ total}$ – obtained by back extrapolation of the high relative pressure region ($\alpha_s < 1$).
[d] $V_{\alpha\ ultra}$ – intercept of the linear range defined the region $p/p^0 \geq 0.02$ ($\phi < 0.7$ nm).
[e] $V_{\alpha\ super}$ – difference between $V_{\alpha\ total}$ and $V_{\alpha\ ultra}$ (0.7 nm < ϕ < 2 nm).

Table 2: XPS atomic percentages for SC800 and SH800.

Sample	**Atomic %** (mmol g^{-1})[a)]	
	C 1s	**O 1s**
SC800	82.3 (64.8)	17.7 (13.9)
SH800	82.8 (65.2)	17.2 (13.5)

[a)] Calculated through: mass C (or O) / mass of sample (calculated from the XPS data) = at.% C 1s (or O1s) / [(at.% C 1s x atomic mass C) + (at.% O 1s x atomic mass O)].

Table 3: Electroactive surface areas (A / cm^2) determined using the Randles-Sevcik equation.

Sample	$[Fe(CN)_6]^{3-/4-}$	$Ru(NH_3)_6]^{3+/2+}$	$Eu^{2+}/^{3+}$
GCE	0.0679 (± 0.0017)	0.0678 (± 0.0004)	0.0447 (± 0.0015)
SC800	0.0776 (± 0.0054)	0.0848 (± 0.0009)	0.0597 (± 0.0010)
SH800	0.0807 (± 0.0013)	0.0840 (± 0.0047)	0.0601 (± 0.0022)

Graphical Abstract

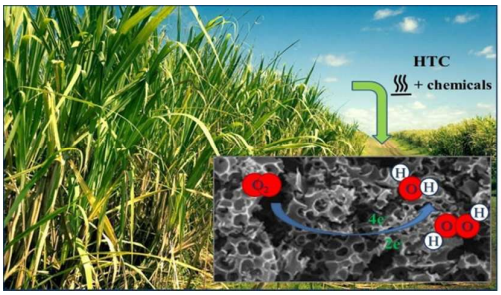

ORR electrocatalysts derived from sugar: activated carbons derived from sucrose showed electrocatalytic activity for the oxygen reduction reaction.